Materials Research. 2018; 21(3): e20170933
DOI: http://dx.doi.org/10.1590/1980-5373-MR-2017-0933

Resistivity Reduction of Nanostructured Undoped Zinc Oxide thin Films for Ag/ZnO Bilayers Using APCVD and Sputtering Techniques

Navid Najafi*[a] *Seyed Mohammad Rozati*[a]

[a]*Department of Physics, University of Guilan, Rasht, Iran*

Received: October 15, 2017; Revised: December 14, 2017; Accepted: February 07, 2018

Nanostructured undoped zinc oxide (ZnO) thin films were deposited using atmospheric pressure chemical vapor deposition (APCVD) on glass substrates using zinc acetate dehydrate [$C_4H_6O_4Zn{\cdot}2H_2O$, ZnAc] in less than 2 minutes for each sample. In order to reduce the resistivity of ZnO films, a very thin layer of Ag was deposited on top of the films via the sputtering method to reduce resistivity from 2.89 to 0.31 Ω.cm, using only a 30Å silver coating. Structural, electrical and optical properties of the resulting bilayers were also investigated. The results show a polycrystalline structure in higher temperatures compared to rather amorphous ones in lower temperatures such as 325°C. The XRD patterns of the optimum polycrystalline films were identified as a hexagonal wurtzite structure of ZnO with the (002) preferred orientation. Also, sheet resistance decreased from 17.8 MΩ/□ to 28.9 KΩ/□ for the temperatures of 325°C to 450°C, respectively. Based on the physical properties of undoped ZnO, substrate temperature is an important factor which affects the crystallite size and modifies electrical parameters. UV-vis measurements revealed a reduction in the transparency of the layers with increasing substrate temperature. A sharp cut-off was observed in ultraviolet regions at around 380 nm.

Keywords: *Zinc oxide, Silver, Chemical vapour deposition (CVD), Sputtering, Electrical resistivity, Bilayers.*

1. Introduction

Zinc oxide (ZnO) is a wide-band-gap (3.37 eV) semiconductor with a large (60 meV) exciton binding energy. It is fairly stable both chemically and physically. Its piezoelectricity and high room temperature electron mobility of 155 $cm^2 V^{-1} s^{-1}$ causes lasing action based on exciton recombination above the room temperature. ZnO has received considerable attention because of its effect in fundamental studies and diverse applications in ultraviolet and blue light-emitting diodes, laser diodes, ferroelectrics, piezoelectrics, gas sensors, field-effect transistors, acoustic wave devices, solars, and so on [1-6]. ZnO has a wurtzite structure, which is, in fact, a hexagonal crystal structure (lattice parameters: a=b=0.32427 nm, c=0.51948 nm), fitting to the space group $P6_3mc$, and is identified by two interconnecting sublattices of O^{2-} and Zn^{2+}, in a way that Zn ions are surrounded by O ions, and vice versa [7].

ZnO is fabricated by various methods such as sputtering [8], spray pyrolysis [9-13], sol-gel [14], thermal oxidation [15], pulsed laser deposition (PLD) [16,17], thermal evaporation [18], spin coating [19], chemical vapor deposition (CVD) [20-22]. ZnO can exist in one, two, or three dimensional structures, giving one of the most considerable collections of diverse particle structures in all materials [23].

Manufacturing as low as possible sheet resistance while maintaining the visible transparency is the main objective of many researches carried out on TCOs. According to Chen et. al [24], there is a lower limit for resistivity (or upper limit for charge carriers' mobility) due to scattering mechanisms. Bellingham et. al [25] suggested 4 x 10^{-7} Ω.m as the absolute TCO resistivity lower limit. The thickness of TCO is very crucial to many applications. Therefore, adding a few nanometers of a second layer of a good conductor (such as a metal) might be a reasonable way to keep the resistivity low without increasing the TCO thickness or losing high percentage of optical transparency. Silver is the best candidate because of having the lowest resistivity among metals [26].

The CVD of films and coatings contains the chemical reactions of reactants in a gaseous phase on or in close vicinity of an already heated substrate surface. This atomistic deposition process can provide highly pure materials with a good structural control at a nanometer or atomic scale level [27]. Atmospheric pressure CVD is an economic method, but has certain difficulties in the process control and most research considerations have been dedicated to low pressure CVD (LPCVD) and sputtering deposition which are, low pressure techniques for deposition. However, because of its potential for mass production, the APCVD of ZnO has been considered [28].

ZnO films manufactured by APCVD with a zinc source such as zinc acetylacetonate ($Zn(C_5H_7O_2)_2$) or zinc acetate are chemically stable in air atmospheric pressure and are used as a precursor instead of diethyl zinc and dimethyl zinc [29]. Atmospheric CVD is advanced by the production of active precursor vapors via gas-phase reactions. They diffuse through a thin hydrodynamic boundary film above the substrate. Because of the low reactivity of oxygen or metal precursors, temperatures above 300°C for the substrate are needed for surface reactions, activating the gas-phase, and having high rates of film growth [30].

*e-mail: smrozati@guilan.ac.ir

2. The Experiment

In this work, we used a homemade CVD apparatus to deposit ZnO films in atmospheric pressure (See Fig. 1) [31].

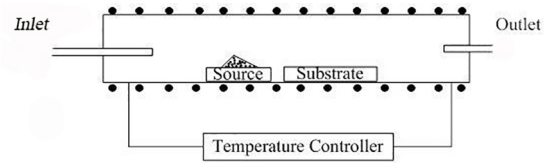

Figure 1. *Air Pressure CVD*

All of the samples were deposited on glass substrates (75 x 25 x 1 mm^3) by the CVD technique in a tube through the oxidation of zinc acetate dihydrate [$C_4H_6O_4Zn{\cdot}2H_2O$, ZnAc] as the precursor. The initial mass of zinc acetate powder was 0.5 g for all the samples and was directly introduced in the reactor. The system contained a horizontal tabular furnace with the diameter of 80 mm and the length of approximately 1 m.

All substrates were put in a detergent solution and then rinsed with deionized water. Next, these glass substrates were ultrasonically cleaned with a mixture of deionized water and HCl acid for 20 minutes. The substrates were rinsed in deionized water again. To prevent the cleaned substrates from oxidization before the deposition, the substrates were heated, while a nitrogen flow was applied to clean the surface of the furnace tube before resuming the deposition process. The deposition duration for each sample was less than 2 minutes depending on the temperature. The less the temperature, the more time it takes to vaporize the fixed amount of 0.5 g as the precursor material. In general, source material, system geometry, and quantity all affect the local vapor pressure of the reactants present at the substrate and, therefore, the properties and morphology of the obtained films [32].

Two sets of experiments were conducted. In Set 1: the temperature of the source material was varied from 325°C to 550°C in steps of 25°C. Air was utilized as the source of oxygen. The zinc acetate dihydrate powder vapor entered the substrate at the atmospheric pressure, and undoped ZnO films were deposited on the substrate. By increasing the temperature from the room temperature, water (H_2O) was vaporised from 50°C, as shown in the reaction Eq. (1). Other products in the gas phase such as acetone, carbon dioxide, and acetic acid started to appear when the temperature reached around 200°C. These materials reached their highest concentration at around 270°C, as shown in Equations (2)- (4). As the temperature rose, ZnO thin films were formed by the chemical reactions below:

$$Zn(CH_3COO)_2 + 2H_2O \longrightarrow Zn(CH_3COO)_2 + 2H_2O\uparrow \quad (1)$$

$$4Zn(CH_3COO)_2 + 2H_2O \longrightarrow Zn_4O(CH_3COO)_6 + 2CH_3COOH\uparrow \quad (2)$$

$$Zn_4O(CH_3COO)_6 + 3H_2O \longrightarrow 4ZnO + 6CH_3COOH\uparrow \quad (3)$$

$$Zn_4O(CH_3COO)_6 \longrightarrow 4ZnO + 6CH_3COCH_3\uparrow + 3CO_2\uparrow \quad (4)$$

Lin et al. considered the thermal process of zinc acetate dihydrate as the dehydration, vaporization/decomposition, and formation of ZnO [33]. The gaseous by-products desorb from the surface, starting to diffuse into the stream and transported by the carrier gas [34]. Then, they must be ventilated by a chemical fume hood [35] in order to be safe for the environment.

In Set 2: a very thin Ag layer of a few angstrom as the second layer was sputtered in the vacuum condition using the DSR sputter vacuum coating sputtering system which employed a 2-inch-diameter magnetron silver target. The sputtering system had a film thickness monitor using a quartz crystal microbalance which was included a 6 MHz quartz crystal.

The transmittance spectra were recorded using a UV-vis spectrophotometer (Perkin-Elmer Lambda 25 UV/vis) in the range of 350-1100 nm. The electrical properties of thin films were measured by the Hall effect and Van der Pauw setup (RH 2010 PhysTech System). X-ray diffraction (XRD) was applied to determine the crystalline quality of the samples using Cu K_α radiation (model Philips PW-1800). Field emission scanning electron microscopy (FESEM) was carried out by a Mira 3-XMU equipped with an energy dispersive X-ray (EDX) system for the morphological analysis of the thin films. The Swanepoel method [36] was employed for thickness measurements of the samples with interference fringes and FESEM cross-section for interference-free thin films.

3. Results and Discussion

3.1 Structural properties

The XRD pattern on the ZnO thin films for different temperatures is demonstrated in Fig. 2. The peaks correlated with the theoretical ZnO patterns of Joint Committee on Powder Diffraction Standards (JCPDS), reference code 01-075-0576, indexed as a hexagonal wurtzite structure with no impurities. In the wurtzite structure of ZnO, the a- and c- axes of the orientation corresponded to (100) and (002) peaks.

At low temperatures, the atomic mobility is low which restricts the crystal growth [37] and a weak peak of (100) is dominated. The lowest sheet resistance is at 450°C in which we have the highest carrier mobility. As Ardyanian et al. [38] suggested, this temperature in the best substrate temperature for ZnO deposition, because atoms have optimum energy for chemical reactions. By increasing the temperature up to 500°C, adatoms receive enough thermal energy and mobility increase which causes the growth of (002) preferred orientation [37]. Hyun et al. [39] stated that the main effect of a change in composition

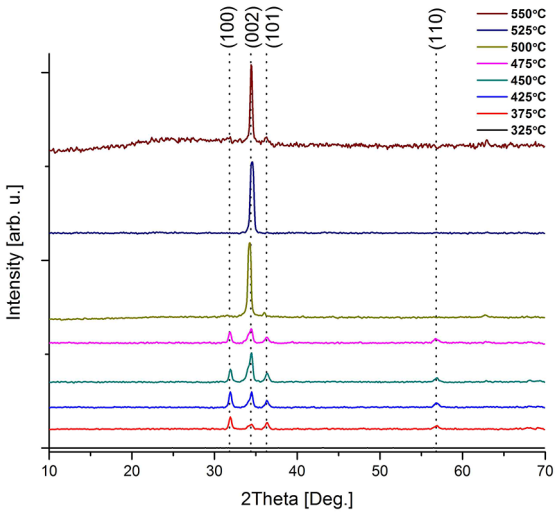

Figure 2. *The XRD pattern of undoped zinc oxide thin films deposited at different substrate temperatures*

from an oxygen-deficient material to a more stoichiometric zinc oxide is the (002) preferred orientation. This causes the sheet resistance to increase for temperatures above 450°C.

The growth rate of each crystallographic plane differs based on crystal orientation and surface energy. The (002) to (100) polar planes ratio of intensity (I_{002}/I_{100}) can affect the photocatalytic activity due to the ZnO polar planes' contribution in the formation of oxygen vacancies [40]. The full width at half maximum (FWHM), crystallite sizes, peak positions, and d-spacing are listed in Table 1 (calculated by the PANalytical X'pert Highscore Plus software). Based on the XRD patterns, the dominant orientation of (002) was at $2\theta \approx 34^{o}$ which is in agreement with a few other works [14,41-44]. The other observed peaks were (100), (101), and (110). Hence, the crystallites were highly oriented with their c-axes which are perpendicular to the substrate plane [45].

Table 1. Structural properties of ZnO thin films prepared at different substrate temperatures

Temperature (°C)	Plane (hkl)	Bragg's angle (2θ)	d-spacing (Å)	FWHM (2θ)	Crystallite size (nm)
	(100)	31.85	2.81	0.16	91.69
375	(002)	34.53	2.60	0.31	46.15
	(101)	36.37	2.47	0.31	46.39
	(100)	31.91	2.80	0.28	52.39
425	(002)	34.50	2.60	0.22	67.12
	(101)	36.32	2.47	0.24	61.84
	(100)	31.92	2.80	0.31	45.84
450	(002)	34.58	2.59	0.26	56.82
	(101)	36.31	2.47	0.20	74.21
	(100)	31.85	2.81	0.28	52.38
475	(002)	34.45	2.60	0.28	52.74
	(101)	36.31	2.47	0.31	46.38
500	(002)	34.11	2.63	0.08	184.45
525	(002)	34.71	2.58	0.08	184.75

Average crystallite size was calculated by the Scherrer's equation (5),

$$D = 0.9\lambda/\beta\cos\theta \tag{5}$$

where λ=1.542 Å is the X-ray wavelength, β is the FWHM of the diffraction in radians, and Θ is the Bragg diffraction angle [46,47].

Inter-planar spacing (d) was measured using the following equation [48]

$$1/d^2 = 4/3\left(\frac{h^2+hk+k^2}{a^2}\right) + l^2/c^2 \tag{6}$$

3.2 Morphological properties

The surface morphology of the thin films was observed using a field emission scanning electron microscope at room temperature. Fig. 3 illustrates FESEM micrographs of ZnO structures deposited on a glass substrate at four different temperatures. By comparing the images, the role of the deposition temperature is vivid. The surface morphology of ZnO thin films grown at a low substrate temperature (325°C) showed small crystallites with a high density. By increasing the temperature to 525°C, the crystallinity of the thin films was enhanced and we obtained the largest crystallites.

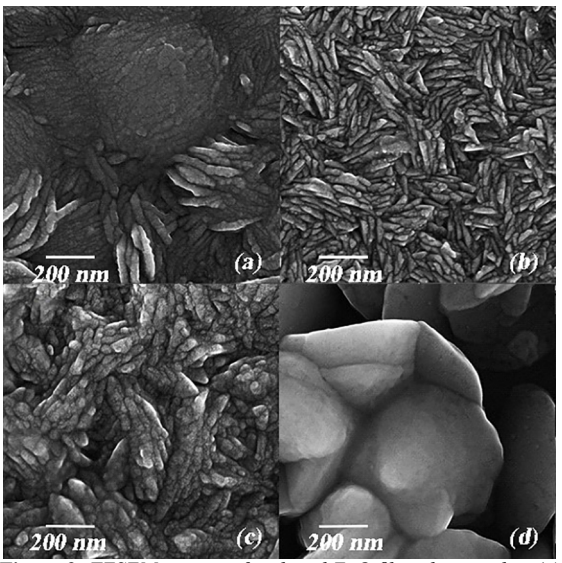

Figure 3. *FESEM images of undoped ZnO films deposited at (a) 325°C, (b) 375°C, (c) 450°C, (d) 525°C degrees*

The morphology of grown ZnO with different thicknesses of Ag nanoparticle coating is depicted in Fig. 4. Slight changes were observed in the microstructure that can be attributed to the role of Ag thickness. As can be seen, the distribution of Ag nanoparticles over the ZnO layer was found to be relatively uniform.

EDX was implemented in different areas of the samples which confirmed the chemical composition of ZnO, as can be seen in Fig. 5. Table 2 shows the quantitative EDX results

for undoped zinc oxide thin films prepared at optimum temperature 450°C. Fig. 6 demonstrates the silver appearance in ZnO/Ag bilayers in the EDX spectrum. Table 3 shows the quantitative EDX results for ZnO/Ag bilayer thin films.

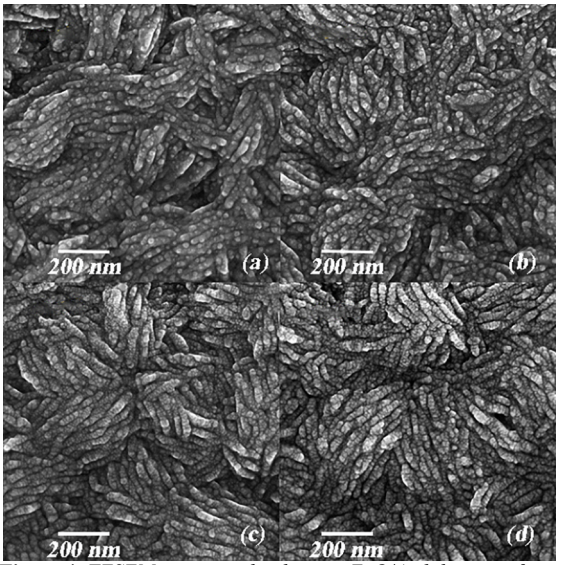

Figure 4. *FESEM micrographs showing ZnO/Ag bilayer surfaces with different Ag thicknesses (a) 5 Å, (b) 10 Å, (c) 20 Å, (d) 30 Å*

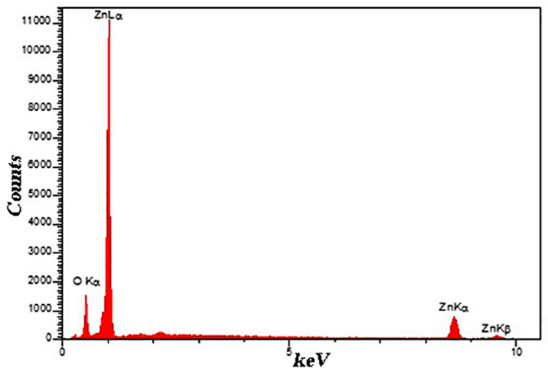

Figure 5. *EDX spectrum measured for undoped zinc oxide thin films prepared at optimum temperature 450°C*

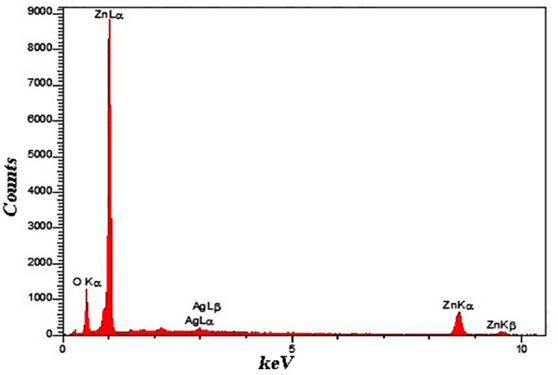

Figure 6. *EDX spectrum measured for ZnO/Ag bilayer thin films*

3.3 Electrical properties

If close to stoichiometry, ZnO films, show very high sheet resistance, while nonstochiometric ZnO films exhibit low sheet resistance. The electrical characteristics of ZnO thin films are mainly dominated by electrons which are generated from Zn interstitial atoms and oxygen vacancies [49]. As in many other semiconductors, the conductivity of ZnO increases with increasing the temperature [50].

Hall effect measurements were conducted using van der Pauw method with the magnetic field of 0.56 T. The samples were cut into square shapes (5 x 5 mm^2). Silver dots were formed as electrodes at the surfaces corners of each sample.

Variations in sheet resistance, resistivity, Hall Co., mobility, and carrier concentration at different substrate temperatures are listed in Table 4. The lowest sheet resistance was achieved at 450°C.

According to Table 5, by taking 450°C as the optimum temperature, films revealed a significant drop in sheet resistance by sputtering a second Ag thin layer on top of the first undoped ZnO layers. As a metal, Ag is a very good conductor but it has a high reflectance. Therefore, we should be very careful about the thickness of the second silver layer because we lose the optical transparency of the films. For this reason, the thickness of the bilayers was limited to 30Å by our sputtering system.

Table 2. Quantitative EDX results for undoped zinc oxide thin films prepared at optimum temperature 450°C.

Elt	Line	Int	Error	K	Kr	W%	A%	ZAF	Ox%	Pk/Bg	Class	LConf	HConf	Cat#
O	Ka	199.7	4.1979	0.1627	0.1315	25.97	58.90	0.5063	0.00	38.77	A	25.30	26.64	0.00
Zn	Ka	216.6	0.7341	0.8373	0.6767	74.03	41.10	0.9140	0.00	26.85	A	72.19	75.87	0.00
				1.0000	0.8081	100.00	100.00		0.00					0.00

Table 3. Quantitative EDX results for ZnO/Ag bilayer thin films.

Elt	Line	Int	Error	K	Kr	W%	A%	ZAF	Ox%	Pk/Bg	Class	LConf	HConf	Cat#
O	Ka	98.9	4.0334	0.1053	0.0895	18.70	48.56	0.4786	0.00	41.49	A	18.02	19.39	0.00
Zn	Ka	175.6	0.6631	0.8865	0.7540	80.42	51.10	0.9376	0.00	27.42	A	78.20	82.63	0.00
Ag	La	6.3	1.8370	0.0082	0.0070	0.88	0.34	0.7963	0.00	2.34	B	0.75	1.00	0.00
				1.0000	0.8505	100.00	100.00		0.00					0.00

Table 4. Electrical properties of ZnO thin films prepared at different substrate temperatures.

Temp. [°C]	Sheet Resistance [Ω/□]	Resistivity [Ω.cm]	Hall Co. [cm^3/As]	Mobility [cm^2/Vs]	Carrier Concentration [cm^{-3}]
325	1.78 x 10^7	2460	-9520	3.88	6.55 x 10^{14}
350	5.88 x 10^6	810	-6480	7.99	9.64 x 10^{14}
375	8.92 x 10^6	1230	-9780	7.93	6.39 x 10^{14}
400	3.44 x 10^6	474	-1270	2.68	4.92 x 10^{15}
425	1.35 x 10^6	186	-147	0.79	4.24 x 10^{16}
450	2.89 x 10^4	3.98	-2.54	0.64	2.46 x 10^{18}
475	8.47 x 10^4	6.11	-10.3	1.69	6.04 x 10^{17}
500	1.20 x 10^6	86.5	-43.5	0.50	1.43 x 10^{17}
525	3.05 x 10^7	2200	-2820	1.28	2.21 x 10^{15}
550	3.05 x 10^7	2200	-13200	6.01	4.73 x 10^{14}

Table 5. Electrical properties of ZnO/Ag bilayers prepared at 450 °C with different Ag thicknesses.

Temp. [°C]	Ag layer thickness [Å]	Sheet Resistance [Ω/□]	Resistivity [Ω.cm]	Hall Co. [cm^3/As]	Mobility [cm^2/Vs]	Carrier Concentration [cm^{-3}]
450	0	2.89 x 10^4	3.98	-2.54	0.64	2.46 x 10^{18}
450	5	6967	0.96	2.10	2.19	2.98 x 10^{18}
450	10	5370	0.74	4.55	6.10	1.37 x 10^{18}
450	20	3411	0.47	4.04	8.65	1.54 x 10^{18}
450	30	2250	0.31	5.88	10.94	1.20 x 10^{18}

Fig. 7 shows sheet resistance, mobility, and carrier concentration variations by substrate temperature.

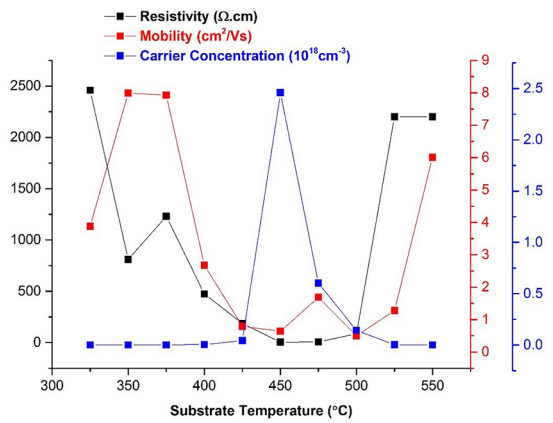

Figure 7. *Variations of resistivity, mobility and carrier concentration versus deposition temperature*

3.4 Optical properties

Fig. 8 illustrates the optical transmittance spectra obtained from ZnO thin films, at the wavelengths ranging from 300-1100 nm, as a function of substrate temperature which plays an important role in film formation. We had a transmittance of about 80% in the visible section of the spectrum from 325°C to the optimum temperature, i.e. 450°C. At higher temperatures, transmittance was reduced and we lost most interference fringes.

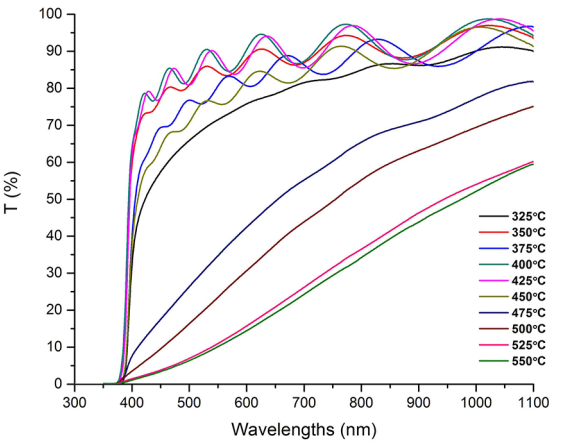

Figure 8. *Optical transmittance spectra for ZnO films deposited with different substrate temperatures*

A sharp cut-off was observed in ultraviolet region at around 380 nm that is due to band edge absorption of ZnO in this area, the monodispersed nature [51], and an almost uniform size of nanoparticles [52] which is also observed by Look [53] and Zhang et al. [54] at 373 nm and 369 nm, respectively.

Fig. 9 demonstrates the optical transmittance spectra resulting from ZnO thin films covered by a few angstroms of Ag with different thicknesses. Ag has a very high reflectance. Therefore, for ZnO/Ag bilayers, as the thickness of Ag is increased, transmittance is reduced.

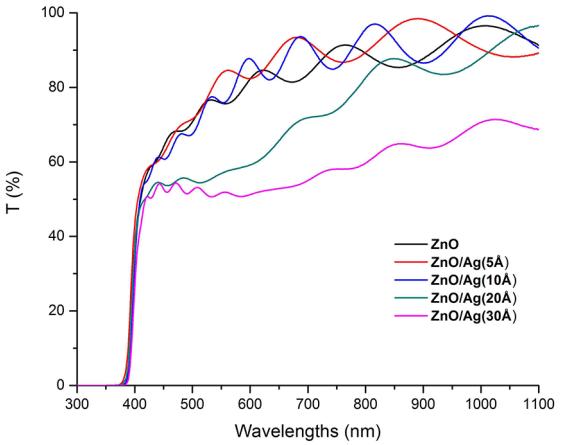

Figure 9. *Optical transmittance spectra for undoped zinc oxide compared to ZnO/Ag bilayers deposited with different Ag thicknesses*

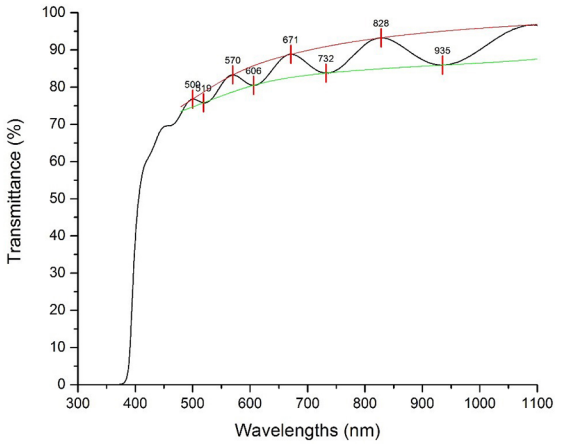

Figure 10. "*Envelope method" graph including extremum values for thickness measurement*

Optical constants such as refractive index, extinction coefficient, and absorption coefficient were calculated using the average transmittance in the visible range. The transmittance of the glass substrate was only T_s = 91.33% in the visible range. Afterwards, the refractive index of the substrate, s=1.540754, was obtained using

$$s = 1/T_S + \left(1/T_S - 1\right)^{1/2} \quad (7)$$

According to the Swanepoel method [36] which is based on the study by Manifacier et al. [55] on making upper and lower envelopes of the transmittance spectrum (see Fig. 10), the refractive index of the film *n* in the transparent, weak, and medium absorption regions can be calculated using

$$n = \left[N + \left(N^2 - s^2\right)^{1/2}\right]^{1/2} \quad (8)$$

where

$$N = 2s/T_m + \left(s^2 + 1\right)/2$$

for the transparent region and

$$N = 2s\left(T_M - T_M\right)/T_M T_m + \left(s^2 + 1\right)/2 \quad (9)$$

for medium and weak absorption regions. T_m and T_M are thecorresponding minimum and maximum transmittances at a certain wavelength, respectively. The thickness of the film was given by:

$$d = \lambda_1 \lambda_2 / 2\left[\lambda_1 n\left(\lambda_2\right) - \lambda_2 n\left(\lambda_1\right)\right] \quad (10)$$

where $n(\lambda_1)$ and $n(\lambda_2)$ are the refractive indices at two adjacent minimums (or maximums) at λ_1 and λ_2, respectively. The fundamental equation for interference fringes is $2nd=m\lambda$ where m is an integer for the maximum and half integer for the minimum.

The calculations of Table 6 correspond to the undoped ZnO sample deposited at 375°C using Eq. (10) and the average thickness of 1378 nm was obtained for this sample. By increasing the deposition temperature, the thickness of the ZnO layers decreases which causes a decrease of grow rate [56]. The thickness of the film influences the optical transmission in which the number of interference fringes and the depth of these fringes depend on the film thickness[57]. Therefore, we performed the Manifacier calculations for the sample with fringes (deposition temperature less than 475°C), resulting an average of 1300nm.

Table 6. The Manifacier's calculations corresponding to the undoped ZnO sample deposited at 375°C using Eq. (10)

λ (nm)	T_M(%)	T_m(%)	s	n	d (nm)
500	77	75	1.54	1.65	2231
519	79	76	1.54	1.69	1339
570	83	79	1.54	1.75	1398
606	86	80	1.54	1.77	1136
671	89	83	1.54	1.79	1283
732	91	84	1.54	1.81	1082
828	93	85	1.54	1.84	1180
935	95	86	1.54	1.85	-

For layers with no or not enough interference fringes in the visible region of the transmission spectra, SEM cross-sections were utilized to measure the thickness of the layers. The average thickness for ZnO layers prepared at 475°C and higher temperatures using SEM cross sections was 721 nm. For these films, the absorption coefficient can be calculated using $\alpha = (1/d)\ln(1/T)$ [44,58-61], $\alpha = (1/d)\ln(100/T)$ [62] or $\alpha = (1/d)\ln(T_0/T)$ [63] equations, where d is the film thickness, and T and T_0 are the transmittance of the ZnO thin film samples and the substrate (glass) without coating, respectively.

Since the Swanepoel method is not valid in the strong absorption region, to determine the absorption coefficient

of the film in the zone, we used Lambert's equation $\alpha = (1/d) \ln T$ [64].

Following the Swanepoel method, the absorption coefficient, α, and extinction coefficient, κ, can be obtained from T_M and T_m, *s* and thickness by the following expressions, respectively [49].

$$\alpha = (1/t) \ln \left[\frac{(n-1)(n-s)\sqrt{T_M/T_m} + 1}{(n+1)(n-s)\sqrt{T_M/T_m} - 1} \right] \quad (11)$$

$$k = \alpha\lambda/4\pi \quad (12)$$

Figs. 11 and 12 depict the absorption and extinction coefficients for samples prepared at different temperatures.

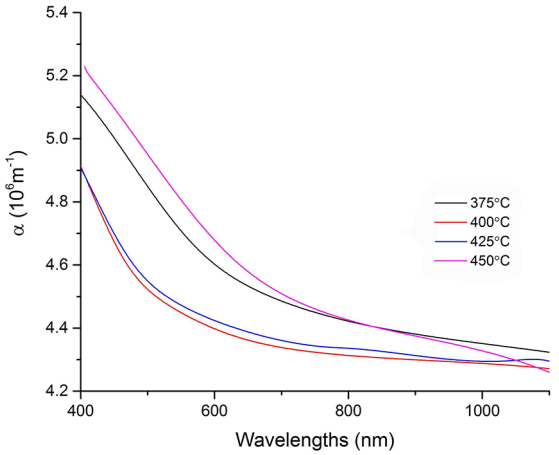

Figure 11. *Variations in absorption coefficient, α, as a function of wavelength for ZnO films at different temperatures*

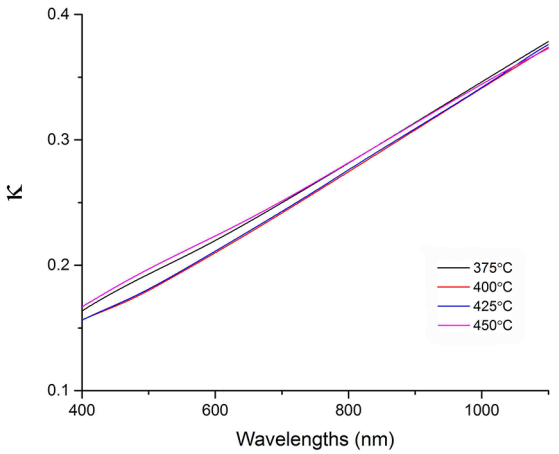

Figure 12. *Variations of extinction coefficient, κ, as a function of wavelength for ZnO films at different temperatures*

Optical transitions in semiconductor materials take place by direct and indirect transitions. The absorption coefficient, α, for direct transitions is expressed by Tauc's relation [65]

$$ahv = B(hv - E_g)^m \quad (13)$$

where B is an energy-independent constant, α is the material's linear absorption coefficient, E_g is the optical band gap and *m* is a constant which regulates the type of optical transitions. For example, in an indirect allowed transition, m=2, for an indirect forbidden transition, m=3, for a direct allowed transition, m=1/2, and for a direct forbidden transition, m=3/2 [48]. In the graph, a straight line is fitted and the extrapolation of this line E(=hv) axis shows the value of the band-gap. The plotted graphs for ZnO thin films with four different substrate temperatures and extrapolated E_g are shown in Fig. 13. The band-gaps of undoped ZnO films were more than 3.2 eV.

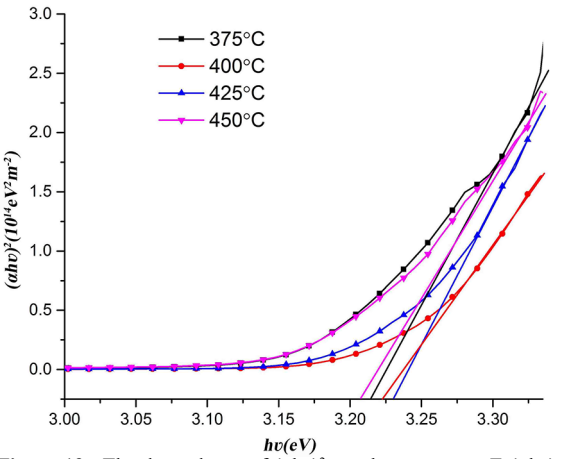

Figure 13. The dependence of $(\alpha h\nu)^2$ on photon energy E (=hν) for different temperatures, from which the optical band gap (E_g) is estimated (Tauc's extrapolation)

4. Conclusion

In this work, we presented the synthesis of ZnO nanostructures prepared by atmospheric pressure CVD on glass substrates at different substrate temperatures in order to achieve the highest optical transparency and electrical conductivity. The optimum set of ZnO films were then used as a substrate for the second Ag layer to be sputtered on top of the first layer. Also, sheet resistance decreased from 17.8 MΩ/□ to 28.9 KΩ/□ for the temperatures of 325°C to 450°C, respectively. Based on the physical properties of undoped ZnO, substrate temperature is an important factor which affects the crystallite size and modifies electrical parameters. UV-vis measurements revealed a reduction in the transparency of the layers with increasing substrate temperature. A sharp cut-off was observed in ultraviolet regions at around 380 nm.

5. Acknowledgements

The authors gratefully acknowledge the research department of the University of Guilan.

6. References

1. Özgür Ü, Alivov YI, Liu C, Teke A, Reshchikov MA, Doğan S, et al. A comprehensive review of ZnO materials and devices. *Journal of Applied Physics*. 2005;98(4):041301. DOI: 10.1063/1.1992666

2. Pawar RC, Kim H, Lee CS. Improved field emission and photocatalysis properties of cacti-like zinc oxide nanostructures *Scripta Materialia*. 2013;68(2):142-145. DOI: 10.1016/j.scriptamat.2012.10.003

3. Yang J, Liu X, Yang L, Wang Y, Zhang Y, Lang J, et al. Effect of different annealing atmospheres on the structure and optical properties of ZnO nanoparticles. *Journal of Alloys and Compounds*. 2009;485(1-2):743-746. DOI: 10.1016/j.jallcom.2009.06.070

4. Li Z, Hu Z, Jiang L, Huang H, Liu F, Zhang X, et al. Synthesis and optical properties of three-dimensional nanowall ZnO film prepared by atmospheric pressure chemical vapor deposition. *Applied Surface Science*. 2012;258(24):10175-10179. DOI: 10.1016/j.apsusc.2012.06.101

5. Liu WW, Yao B, Li YF, Li BH, Zhang ZZ, Shan CX, et al. Structure, luminescence and electrical properties of ZnO thin films annealed in H_2 and H_2O ambient: A comparative study. *Thin Solid Films*. 2010;518(14):3923-3928. DOI: 10.1016/j.tsf.2009.12.099

6. Xu J, Pan Q, Shun Y, Tian Z. Grain size control and gas sensing properties of ZnO gas sensor. *Sensors and Actuators B: Chemical*. 2000;66(1-3):277-279. DOI: 10.1016/S0925-4005(00)00381-6

7. Benramache S, Belahssen O, Arif A, Guettaf A. A correlation for crystallite size of undoped ZnO thin film with the band gap energy - precursor molarity - substrate temperature. *Optik - International Journal for Light and Electron Optics*. 2014;125(3):1303-1306. DOI: 10.1016/j.ijleo.2013.08.015

8. Axelevitch A, Gorenstein B, Darawshe H, Golan G. Investigation of thin solid ZnO films prepared by sputtering. *Thin Solid Films*. 2010;518(16):4520-4524. DOI: 10.1016/j.tsf.2009.12.021

9. Lehraki N, Aida MS, Abed S, Attaf N, Attaf A, Poulain M. ZnO thin films deposition by spray pyrolysis: Influence of precursor solution properties. *Current Applied Physics*. 2012;12(5):1283-1287. DOI: 10.1016/j.cap.2012.03.012

10. Mahajan CM, Takwale MG. Intermittent spray pyrolytic growth of nanocrystalline and highly oriented transparent conducting ZnO thin films: Effect of solution spray rate. *Journal of Alloys and Compounds*. 2014;584:128-135. DOI: 10.1016/j.jallcom.2013.08.136

11. Bacaksiz E, Yilmaz S, Parlak M, Varilci A, Altunbas M. Effects of annealing temperature on the structural and optical properties of ZnO hexagonal pyramids. *Journal of Alloys and Compounds*. 2009;478(1-2):367-370. DOI: 10.1016/j.jallcom.2008.11.025

12. Baneto M, Enesca A, Lare Y, Jondo K, Napo K, Duta A. Effect of precursor concentration on structural, morphological and opto-electric properties of ZnO thin films prepared by spray pyrolysis. *Ceramics International*. 2014;40(6):8397-8404. DOI: 10.1016/j.ceramint.2014.01.048

13. Nunes P, Fernandes B, Fortunato E, Vilarinho P, Martins R. Performances presented by zinc oxide thin films deposited by spray pyrolysis. *Thin Solid Films*. 1999;337(1-2):176-179. DOI: 10.1016/S0040-6090(98)01394-7

14. Caglar M, Ruzgar S. Influence of the deposition temperature on the physical properties of high electron mobility ZnO films by sol-gel process. *Journal of Alloys and Compounds*. 2015;644:101-105. DOI: 10.1016/j.jallcom.2015.04.167

15. Girtan M, Rusu GG, Dabos-Seignon S, Rusu M. Structural and electrical properties of zinc oxides thin films prepared by thermal oxidation. *Applied Surface Science*. 2008;254(13):4179-4185. DOI: 10.1016/j.apsusc.2007.12.055

16. Wei XQ, Zhang ZG, Liu M, Chen CS, Sun G, Xue CS, et al. Annealing effect on the microstructure and photoluminescence of ZnO thin films. *Materials Chemistry and Physics*. 2007;101(2-3):285-290. DOI: 10.1016/j.matchemphys.2006.05.005

17. Pe´rez-Casero R, Gutie´rrez-Llorente A, Pons-Y-Moll O, Seiler W, Defourneau RM, Defourneau D, et al. Er-doped ZnO thin films grown by pulsed-laser deposition. *Journal of Applied Physics*. 2005;97(5):054905. DOI: 10.1063/1.1858058

18. Yang XX, Lei W, Zhang XB, Wang BP, Li C, Hou K, et al. Growth and optical and field emission properties of flower-like ZnO nanostructures with hexagonal crown. *Thin Solid Films*. 2009;517(15):4385-4389. DOI: 10.1016/j.tsf.2009.01.056

19. Berber M, Bulto V, Kliß R, Hahn H. Transparent nanocrystalline ZnO films prepared by spin coating. *Scripta Materialia*. 2005;53(5):547-551. DOI: 10.1016/j.scriptamat.2005.04.047

20. Kashiwaba Y, Katahira F, Haga K, Sekiguchi T, Watanabe H. Hetero-epitaxial growth of ZnO thin films by atmospheric pressure CVD method. *Journal of Crystal Growth*. 2000;221(1-4):431-434. DOI: 10.1016/S0022-0248(00)00729-6

21. Yoo YZ, Kim SH, Yoon GS, Choi EH, Park JW, Park JH, et al. Development of tilted hexagonal platelet ZnO using atmospheric pressure chemical vapor deposition and investigation of its growth mechanism. *Applied Physics Letters*. 2012;100(6):061909. DOI: 10.1063/1.3681163

22. de Graaf A, van Deelen J, Poodt P, van Mol T, Spee K, Grob F, et al. Development of atmospheric pressure CVD processes for highquality transparent conductive oxides. *Energy Procedia*. 2010;2(1):41-48. DOI: 10.1016/j.egypro.2010.07.008

23. Kolodziejczak-Radzimska A, Jesionowski T. Zinc Oxide-From Synthesis to Application: A Review. *Materials*. 2014;7(4):2833-2881. DOI: 10.3390/ma7042833

24. Chen M, Pei ZL, Wang X, Yu YH, Liu XH, Sun C, et al. Intrinsic limit of electrical properties of transparent conductive oxide films. *Journal of Physics D: Applied Physics*. 2000;33(20):2538-2548. DOI: 10.1088/0022-3727/33/20/304

25. Bellingham JR, Phillips WA, Adkins CJ. Intrinsic performance limits in transparent conducting oxides. *Journal of Materials Science Letters*. 1992;11(5):263-265. DOI: 10.1007/bf00729407

26. Lide DR, ed. *Handbook of Chemistry and Physics*. Boca Raton: CRC Press; 1997.

27. Choy KL. Chemical vapour deposition of coatings. *Progress in Materials Science*. 2003;48(2):57-170. DOI: 10.1016/S0079-6425(01)00009-3

28. van Deelen J, Illiberi A, Kniknie B, Beckers EHA, Simons PJPM, Lankhorst A. Atmospheric pressure chemical vapor deposition of ZnO: Process modeling and experiments. *Thin Solid Films*. 2014;555:163-168. DOI: 10.1016/j.tsf.2013.08.009

29. Pacio M, Juárez H, Escalante G, García G, Díaz T, Rosendo E. Study of (1 0 0) orientated ZnO films by APCVD system. *Materials Science and Engineering: B*. 2010;74(1-3):38-41. DOI: 10.1016/j.mseb.2010.04.030

30. Illiberi A, Poodt P, Bolt PJ, Roozeboom F. Recent Advances in Atmospheric Vapor-Phase Deposition of Transparent and Conductive Zinc Oxide. *Chemical Vapor Deposition*. 2014;20(7-8-9):234-242. DOI: 10.1002/cvde.201400056

31. Maleki M, Rozati SM. Structural, electrical and optical properties of transparent conducting SnO_2 films: effect of the oxygen flow rate. *Physica Scripta*. 2012;86(1):015801. DOI: 10.1088/0031-8949/86/01/015801

32. Djurišić AB, Ng AMC, Chen XY. ZnO nanostructures for optoelectronics: Material properties and device applications. *Progress in Quantum Electronics*. 2010;34(4):191-259. DOI: 10.1016/j.pquantelec.2010.04.001

33. Lin CC, Li YY. Synthesis of ZnO nanowires by thermal decomposition of zinc acetate dihydrate. *Materials Chemistry and Physics*. 2009;113(1):334-337. DOI: 10.1016/j.matchemphys.2008.07.070

34. Gomez JL, Tigli O. Zinc oxide nanostructures: from growth to application. *Journal of Materials Science*. 2012;48(2):612-624. DOI: 10.1007/s10853-012-6938-5

35. Paraguay D F, Estrada L W, Acosta N DR, Andrade E, Miki-Yoshida M. Growth, structure and optical characterization of high quality ZnO thin films obtained by spray pyrolysis. *Thin Solid Films*. 1999;350(1-2):192-202. DOI: 10.1016/s0040-6090(99)00050-4

36. Swanepoel R. Determination of the thickness and optical constants of amorphous silicon. *Journal of Physics E: Scientific Instruments*. 1983;16(12):1214. DOI: 10.1088/0022-3735/16/12/023

37. Kang SJ, Joung YH, Shin HH, Yoon YS. Effect of substrate temperature on structural, optical and electrical properties of ZnO thin films deposited by pulsed laser deposition. *Journal of Materials Science: Materials in Electronics*. 2008;19(11):1073-1078. DOI: 10.1007/s10854-007-9469-0

38. Ardyanian M, Bagheri-Mohagheghi MM, Sedigh N. Determination of the optimal parameters for the fabrication of ZnO thin films prepared by spray pyrolysis method. *Pramana*. 2012;78(4):625-634. DOI: 10.1007/s12043-011-0257-2

39. Yoon KH, Choi JW, Lee DH. Characteristics of ZnO thin films deposited onto Al/Si substrates by r.f. magnetron sputtering. *Thin Solid Films*. 1997;302(1-2):116-121. DOI: 10.1016/s0040-6090(96)09568-5

40. Hamdam Momen M, Amadeh A, Heydarzadeh Sohi M, Moghanlou Y. Photocatalytic properties of ZnO nanostructures grown via a novel atmospheric pressure solution evaporation method. *Materials Science and Engineering: B*. 2014;190:66-74. DOI: 10.1016/j.mseb.2014.09.002

41. Park NK, Lee YJ, Yoon SH, Han GB, Ryu SO, Lee TJ, et al. The epitaxial growth of ZnO nanowires for optical devices by a modified thermal evaporation method. *Scripta Materialia*. 2008;59(3):328-331. DOI: 10.1016/j.scriptamat.2008.03.042

42. Lupan O, Pauporté T, Chow L, Viana B, Pellé F, Ono LK, et al. Effects of annealing on properties of ZnO thin films prepared by electrochemical deposition in chloride medium. *Applied Surface Science*. 2010;256(6):1895-1907. DOI: 10.1016/j.apsusc.2009.10.032

43. Lu JG, Kawaharamura T, Nishinaka H, Kamada Y, Ohshima T, Fujita S. Zno-based thin films synthesized by atmospheric pressure mist chemical vapor deposition. *Journal of Crystal Growth*. 2007;299(1):1-10. DOI: 10.1016/j.jcrysgro.2006.10.251

44. Gümüz C, Ozkendir OM, Kavak H, Ufuktepe Y. Structural and optical properties of zinc oxide thin films prepared by spray pyrolysis method. *Journal of Optoelectronics and Advanced Materials*. 2006;8(1):299-303.

45. Ilican S, Caglar M, Caglar Y. Determination of the thickness and optical constants of transparent indium-doped ZnO thin films by the envelope method. *Materials Science-Poland*. 2007;25(3):709-718.

46. Tsai YZ, Wang NF, Tsai CL. Fluorine-doped ZnO transparent conducting thin films prepared by radio frequency magnetron sputtering. *Thin Solid Films*. 2010;518(17):4955-4959. DOI: 10.1016/j.tsf.2010.03.086

47. Cullity BD, Stock SR. *Elements of X-Ray Diffraction*. 3rd ed. Harlow: Pearson; 2001.

48. Yakuphanoglu F. Electrical characterization and device characterization of ZnO microring shaped films by sol-gel method. *Journal of Alloys and Compounds*. 2010;507(1):184-189. DOI: 10.1016/j.jallcom.2010.07.151

49. Bhat JS, Patil AS, Swami N, Mulimani BG, Gayathri BR, Deshpande NG, et al. Electron irradiation effects on electrical and optical properties of sol-gel prepared ZnO films. *Journal of Applied Physics*. 2010;108(4):043513. DOI: 10.1063/1.3452333

50. Moezzi A, McDonagh AM, Cortie MB. Zinc oxide particles: Synthesis, properties and applications. *Chemical Engineering Journal*. 2012;185-186:1-22. DOI: 10.1016/j.cej.2012.01.076

51. Talam S, Karumuri SR, Gunnam N. Synthesis, Characterization, and Spectroscopic Properties of ZnO Nanoparticles. *ISRN Nanotechnology*. 2012;2012:372505. DOI: 10.5402/2012/372505

52. Alwan RM, Kadhim QA, Sahan KM, Ali RA, Mahdi RJ, Kassim NA, et al. Synthesis of Zinc Oxide Nanoparticles via Sol - Gel Route and Their Characterization. *Nanoscience and Nanotechnology*. 2015;5(1):1-6. DOI: 10.5923/j.nn.20150501.01

53. Look DC. Recent advances in ZnO materials and devices. *Materials Science and Engineering: B*. 2001;80(1-3):383-387. DOI: 10.1016/S0921-5107(00)00604-8

54. Zhang XL, Hui KS, Hui KN. High photo-responsivity ZnO UV detectors fabricated by RF reactive sputtering. *Materials Research Bulletin*. 2013;48(2):305-309. DOI: 10.1016/j.materresbull.2012.10.030

55. Manifacier JC, Gasiot J, Fillard JP. A simple method for the determination of the optical constants n, k and the thickness of a weakly absorbing thin film. *Journal of Physics E: Scientific Instruments*. 1976;9(11):1002. DOI: 10.1088/0022-3735/9/11/032

56. Bensmaine S, Benyoucef B. Effect of the Temperature on ZnO Thin Films Deposited by r.f. Magnetron. *Physics Procedia*. 2014;55:144-149. DOI: 10.1016/j.phpro.2014.07.021

57. Gungor T, Gungor E, Saka B. Fast and interference fringe independent optical characterization of zinc oxide nano thin films using model-based genetic algorithm for optoelectronic applications. *Nanomaterials and Nanotechnology*. 2016;6:1-7. DOI: 10.1177/1847980416673785

58. Joseph B, Manoj PK, Vaidyan VK. Studies on the structural, electrical and optical properties of Al-doped ZnO thin films prepared by chemical spray deposition. *Ceramics International*. 2006;32(5):487-493. DOI: 10.1016/j.ceramint.2005.03.029

59. Thonglem S, Intatha U, Eitssayeam S. Effect of magnesium and fluorine dopants on properties of ZnO thin films. *Ceramics International*. 2015;41(Suppl 1):S331-S336. DOI: 10.1016/j.ceramint.2015.03.215

60. Wu M, Yu S, Chen G, He L, Yang L, Zhang W. Structural, optical, and electrical properties of Mo-doped ZnO thin films prepared by magnetron sputtering. *Applied Surface Science*. 2015;324:791-796. DOI: 10.1016/j.apsusc.2014.11.039

61. Hu D, Liu X, Deng S, Liu Y, Feng Z, Han B, et al. Structural and optical properties of Mn-doped ZnO nanocrystalline thin films with the different dopant concentrations. *Physica E: Low-dimensional Systems and Nanostructures*. 2014;61:14-22. DOI: 10.1016/j.physe.2014.03.007

62. Zunke I, Heft A, Schäfer P, Haidu F, Lehmann D, Grünler B, et al. Conductive zinc oxide thin film coatings by combustion chemical vapour deposition at atmospheric pressure. *Thin Solid Films*. 2013;532:50-55. DOI: 10.1016/j.tsf.2012.11.151

63. Shirazi M, Hosseinnejad MT, Zendehnam A, Ghoranneviss M, Reza Etaati G. Synthesis and characterization of nanostructured ZnO multilayer grown by DC magnetron sputtering. *Journal of Alloys and Compounds*. 2014;602:108-116. DOI: 10.1016/j.jallcom.2014.03.029

64. Choi YJ, Park HH. A simple approach to the fabrication of fluorine-doped zinc oxide thin films by atomic layer deposition at low temperatures and an investigation into the growth mode. *Journal of Materials Chemistry C*. 2014;2(1):98-108. DOI: 10.1039/C3TC31478B

65. Tauc J, Menth A. States in the gap. *Journal of Non-Crystalline Solids*. 1972;8-10(1972):569-585. DOI: 10.1016/0022-3093(72)90194-9